Experimentally minimized beam emittance from an *L*-band photoinjector

M. Krasilnikov,* F. Stephan, G. Asova,† H.-J. Grabosch, M. Groß, L. Hakobyan, I. Isaev, Y. Ivanisenko, L. Jachmann, M. Khojoyan,‡ G. Klemz, W. Köhler, M. Mahgoub, D. Malyutin, M. Nozdrin,§ A. Oppelt, M. Otevrel, B. Petrosyan, S. Rimjaem,‖ A. Shapovalov, G. Vashchenko, S. Weidinger, and R. Wenndorff
Deutsches Elektronen Synchrotron DESY, Platanenallee 6, 15738 Zeuthen, Germany

K. Flöttmann, M. Hoffmann, S. Lederer, H. Schlarb, and S. Schreiber
Deutsches Elektronen-Synchrotron DESY, Notkestraße 85, 22607 Hamburg, Germany

I. Templin and I. Will
Max-Born-Institut, Max-Born-Strasse 2A, 12489 Berlin, Germany

V. Paramonov
Institute for Nuclear Research, 60th October Anniversary Prospect, 7A, 117312 Moscow, Russia

D. Richter
Helmholtz-Zentrum Berlin, Hahn-Meitner-Platz 1, 14109 Berlin, Germany
(Received 18 June 2012; published 3 October 2012)

High brightness electron sources for linac based free-electron lasers (FELs) are being developed at the Photo Injector Test facility at DESY, Zeuthen site (PITZ). Production of electron bunches with extremely small transverse emittance is the focus of the PITZ scientific program. The photoinjector optimization in 2008–2009 for a bunch charge of 1, 0.5, 0.25, and 0.1 nC resulted in measured emittance values which are beyond the requirements of the European XFEL [S. Rimjaem *et al.*, Nucl. Instrum. Methods Phys. Res., Sect. A **671**, 62 (2012)]. Several essential modifications were commissioned in 2010–2011 at PITZ, resulting in further improvement of the photoinjector performance. Significant improvement of the rf gun phase stability is a major contribution in the reduction of the measured transverse emittance. The old TESLA prototype booster was replaced by a new cut disk structure cavity. This allows acceleration of the electron beam to higher energies and supports much higher flexibility for stable booster operation as well as for longer rf pulses which is of vital importance especially for the emittance optimization of low charge bunches. The transverse phase space of the electron beam was optimized at PITZ for bunch charges in the range between 0.02 and 2 nC, where the quality of the beam measurements was preserved by utilizing long pulse train operation. The experimental optimization yielded worldwide unprecedented low normalized emittance beams in the whole charge range studied.

DOI: 10.1103/PhysRevSTAB.15.100701 PACS numbers: 29.25.Bx, 41.60.Cr, 52.59.Sa, 29.27.Fh

I. INTRODUCTION

The availability of a high brightness electron source is one of the key issues for successful operation of linac based free-electron lasers (FELs) like the Free-electron Laser in Hamburg, FLASH [1], and the European X-ray Free-Electron Laser, European XFEL [2]. The self-amplified spontaneous emission (SASE) of the FEL process requires an extremely high space charge density of the radiating electron bunches implying high peak current, low energy spread, and small transverse emittance of the electron beam [3]. The latter property cannot be improved in a linac and thus the emittance has to be minimized already in the injector. The Photo Injector Test facility at DESY, Zeuthen site (PITZ), aims to produce electron bunches with extremely small transverse emittance. In 2007 it was shown for the first time that the stringent requirement on beam emittance for the European XFEL of 0.9 mm mrad at 1 nC bunch charge in the injector can be reached if 10% of the total amount of electrons are removed from the outer area of the measured transverse phase space, which anyhow are not expected to contribute to the lasing in the FEL process [4]. Further improved measured emittance values have been demonstrated in 2008–2009 at PITZ for various bunch charge levels—from 0.1 nC to the nominal 1 nC [5].

*Corresponding author.
mikhail.krasilnikov@desy.de
†Currently at INRNE, Sofia, Bulgaria.
‡On leave from YERPHI, Yerevan, Armenia.
§On leave from JINR, Dubna, Russia.
‖Currently at Chiang Mai University, Chiang Mai, Thailand.

The obtained measured 100% rms emittance (no charge cut on the phase space) of 0.89 mm mrad for 1 nC beams is even better than the European XFEL requirements [2]. The main limiting factor at that run period was the rf gun phase instability resulting in a measured emittance growth especially for low charge bunches. The installation of a 10-MW in-vacuum directional coupler improved the gun phase stability by an order of magnitude. Besides this a new booster cavity was installed and commissioned at PITZ allowing a significant beam energy increase and substantial improvement in long pulse train operation. Small improvements in the electron beam line like elimination of magnetizable components also led to better photoinjector performance. These upgrades resulted in ~30% further emittance reduction. Also the bunch charge range has been extended in both directions, so the beam emittance has been optimized for bunch charges from 0.02 to 2 nC. The results obtained are setting a new benchmark for experimentally optimizing photoinjector performance in the whole charge range.

II. PITZ SETUP IN 2010–2011

The PITZ setup in 2010–2011 (Fig. 1) consists of a photocathode rf gun, a normal conducting booster cavity, and various systems for cathode laser and electron beam diagnostics. The PITZ rf gun delivers electron bunches with up to several nC charge and a maximum momentum of up to 7 MeV/c. The low energy diagnostic section includes a dispersive arm to measure beam energy and three screen stations in a straight section followed by an accelerating cavity called booster. The distance from the cathode to the first iris of the booster cavity is 3.24 m. The final maximum momentum after the booster was measured to be 24.5 MeV/c. The high energy diagnostic section contains a variety of beam measurement devices.

Several significant modifications in the PITZ linac have been implemented since 2009 when a previous injector optimization run took place [5]. In the following the main upgrades are shortly described.

A. RF gun system

The PITZ gun is a 1.6 cell L-band normal conducting rf cavity with a Cs_2Te photocathode. The main solenoid is centered at 0.276 m from the cathode plane, the bucking solenoid for compensation of the longitudinal magnetic field at the cathode is placed behind the gun cavity. The cathode laser is coupled to the photocathode by means of a vacuum mirror installed in a diagnostic cross 0.72 m downstream of the cathode plane.

The gun cavity (gun prototype 4.2) used in the 2008–2009 run period showed a remarkably low dark current level [6] and very good performance in terms of beam emittance [5]. The gun was moved to the FLASH injector and put into FEL user operation. Another gun cavity (gun prototype 4.1) was installed and conditioned at PITZ in 2010 [7]. It should be noticed that both gun cavities (gun prototypes 4.1 and 4.2) have the same design and were produced in one series. The same tuning and dry-ice sublimation impulse cleaning procedure [8] was applied to both cavities. The tuning procedure by slightly deforming the cavity end walls in order to reach the desired mean resonance frequency of 1.3 GHz resulted in a field balance (ratio of the field amplitude at the cathode to the full cell peak field) of 1.08 for the gun prototype 4.1 whereas 1.05 was obtained for the gun prototype 4.2.

The present PITZ gun (prototype 4.1) was conditioned up to a peak power of ~6 MW—the maximum power available from the klystron at the gun cavity. The maximum average rf power in the gun achieved in 2011 was 42 kW with 700 μs rf pulse duration at 10 Hz repetition rate. The typical rf pulse length used during emittance studies was up to 300 μs.

The rf feed of the gun is realized using a 10 MW multibeam (MB) klystron (Fig. 2). The klystron supplies the power via two waveguide arms. A T combiner is installed in the rf gun vicinity and serves to superpose waves from these two arms to feed the gun cavity. A phase shifter in one of the waveguides is used to match amplitudes and phases of the mixing waves. The combined wave is fed through a rotationally symmetric coaxial coupler into the rf gun. The gun operation utilizing this rf system allows one

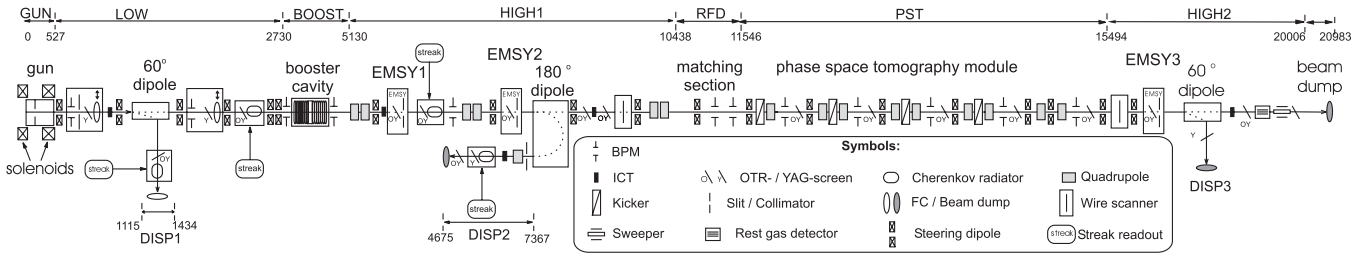

FIG. 1. Schematic diagram of the 2010–2011 PITZ electron beam line including electron gun and CDS booster cavity. Diagnostics is presented by dispersive arms (DISP1,2,3), stations with optical transition radiation and YAG screens (O/Y), and emittance measurement system stations (EMSY1,2,3). Coordinates (z positions) with respect to (w.r.t.) the cathode plane are given in mm.

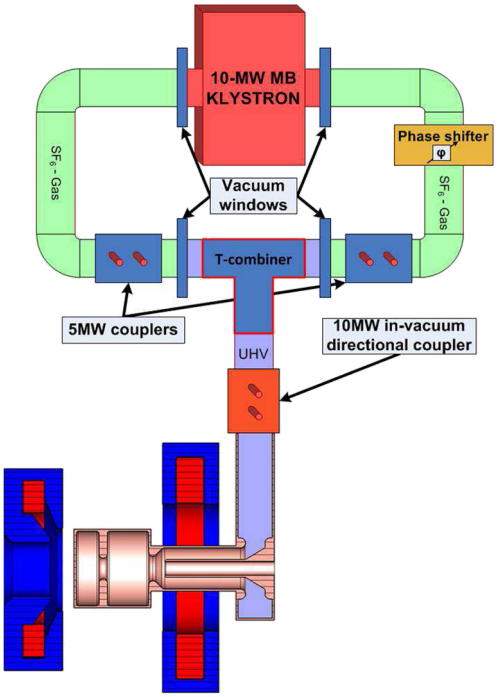

FIG. 2. Schematic diagram of the rf gun power supply.

to reach a nominal peak electric field of ~60 MV/m at the cathode. To isolate the ultrahigh vacuum gun cavity from the SF_6-filled waveguides, two rf windows are installed in front of the input ports of the T combiner.

Compared to the previous setup the present rf feed regulation has been significantly improved by the installation of a 10 MW in-vacuum directional coupler [9] right after the T combiner (Fig. 2). Before this upgrade the rf regulation was realized by a solution based on the signals from the two directional couplers installed before the input port of the T combiner (so-called 5 MW couplers in Fig. 2). The possible cross talk of the T combiner input ports, reflection from the rf windows, changing tuning of the gun cavity due to water cooling stabilization imperfections, and finite directivity of the coupler pickups make the task of rf power regulation in the gun extremely complicated. Because of that problem no efficient feedback could be realized in the previous PITZ gun setup resulting in a significant jitter of the rf phase [5]. The feedback in the current setup was implemented based on signals from the 10 MW in-vacuum directional coupler resulting in a phase stability improvement by more than 1 order of magnitude [9]. Besides shot-to-shot phase jitter reduction, the flatness of the phase profile within the rf pulse has been significantly improved. This is of great importance especially for long electron bunch train operation. A typical phase slope before the upgrade was ~0.12 deg/μs (Fig. 3). This implies, e.g., that the first and the hundredth pulse see an rf phase difference of ~12 deg. The correction implemented in 2011 resulted in an almost zero phase slope and therefore in almost identical phase for all bunches in the pulse train. Results of direct phase shot-to-shot jitter measurements are shown in Fig. 3 with histograms for the first bunch in a bunch train. The rms phase jitter is decreased from 2.5 to 0.1 deg.

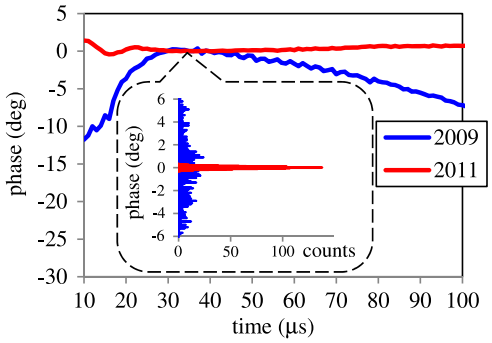

FIG. 3. The rf gun phase stability and jitter before and after the upgrade. The main diagram shows the phase distribution within an rf pulse. The inserted histograms are illustrating shot-to-shot phase jitter measurements performed for the first bunch location within the rf pulse.

B. CDS booster

Until 2010 a normal conducting TESLA prototype cavity was used as a booster cavity at PITZ. It had a side coupling slot in the middle cell, disturbing the rotational field symmetry. Because of a rather poor cooling system, the TESLA booster was strongly restricted in the rf pulse length at higher peak powers; any interlock recovery took a long time. This significantly complicated emittance measurements, especially for longer pulse trains as required to measure emittance of low charge beams. The maximum energy gain of about 10 MeV was available only for short rf pulses (less than 50 μs).

A new booster cavity based on a cut disk structure (CDS) developed by INR (Moscow) was installed and commissioned in 2010 [10]. It provides an almost doubled energy gain compared to the old TESLA booster. The CDS booster is specially designed for PITZ and supports long pulse train operation at maximum peak rf power. Currently a maximum final beam momentum of 24.5 MeV/c has been obtained. Figure 4 illustrates the beam momentum measured after the gun and after the booster as a function of the peak rf power in the gun or booster, respectively. These measurements were performed by operation of gun and booster cavities at the phase of the maximum mean momentum gain (MMMG). Corresponding curves for the gun prototype 4.2 and the old TESLA booster are shown as well. The maximum attainable beam momentum after the gun of up to almost 7 MeV/c was measured for both guns.

C. Photocathode laser

The photocathode laser system was developed by the Max-Born Institute. It was installed in its original configuration at PITZ in 2008 and upgraded with a new Yb:YAG

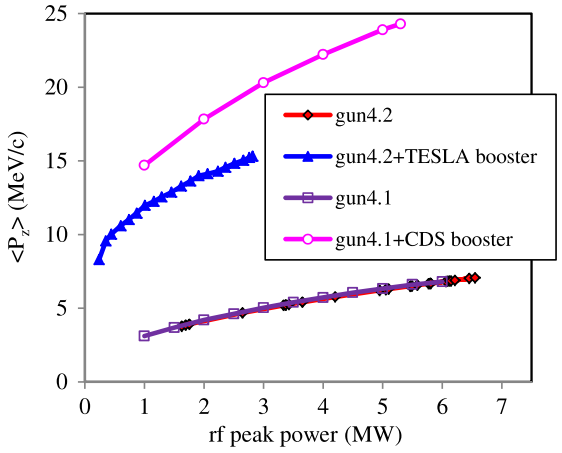

FIG. 4. Electron beam mean momentum as a function of the peak rf power in the gun and booster. For the momentum measurements after the booster the gun was operated at the maximum mean momentum gain.

based pulse train oscillator in 2010. Laser pulse trains with up to 800 micropulses and 1 μs spacing between the pulses of the train can be produced at 10 Hz repetition rate.

A longitudinal pulse shaper is based on 13 birefringent crystals to transform the initial short Gaussian pulse into a temporal flattop profile with rise and fall times as short as ~2 ps and a maximum pulse length of 24 ps FWHM [11].

An Yb:YAG regenerative amplifier and a two-stage Yb:YAG booster amplifier together with frequency conversion crystals provide UV output pulses with a wavelength of 257 nm and a maximum energy of ~10 μJ per micropulse.

An optical sampling system (OSS) based on optical cross-correlation technique is used at PITZ to measure the temporal profile of the UV output pulses. Its resolution is better than 1 ps [11].

Laser temporal profiles with ~21 ps FWHM and 2–3 ps rise and fall time were used for the photoinjector optimization. Figure 5 shows typical temporal laser profiles measured while the best emittance for a given bunch charge was obtained. These profiles were measured within several months of the run; several small readjustments of the pulse shaper were done in order to compensate a slow drift of the pulse profile.

The transverse distribution of the cathode laser pulse is another major factor impacting the transverse emittance. Transverse pulse shaping was realized by cutting off the central part of the laser spot with a beam shaping aperture (BSA) and its consequent imaging onto the photocathode. Several plates with fixed sets of BSAs were installed in the laser beam line. The pool of the laser BSAs available from three plates covers diameters from 0.05 to 0.7 mm with a step of 0.05 mm and additionally includes diameters of 0.8, 1.0, 1.2, 1.5, 1.8, 2.0, 2.5, and 3.0 mm. Remotely controlled positioning of the chosen BSA enabled fine adjustment of the transverse shape of the laser pulse having a homogeneous radial distribution as a goal. Remotely controllable mirrors were tuned for each optimization step centering the laser spot at the photocathode, thereby aligning the laser spot center of mass with the electrical axis of the gun cavity.

The transverse distribution of the cathode laser is monitored with a UV sensitive CCD camera placed at a location which is optically equivalent to the real cathode position. Typical transverse distributions are shown in Fig. 6 for various laser BSAs.

The inhomogeneity of the laser transverse distributions for larger spot sizes are mainly caused by inhomogeneities

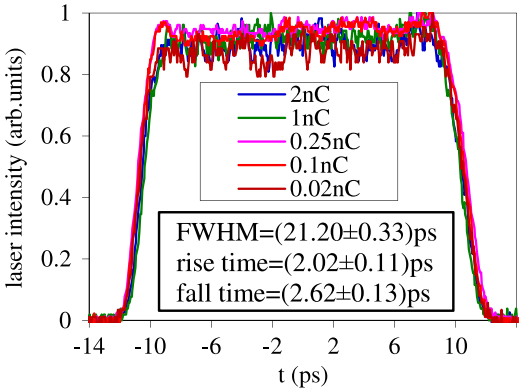

FIG. 5. Photocathode laser pulse temporal profiles measured with the OSS. The different curves correspond to the laser pulse shape detected while the best emittance for the given bunch charge was measured. The statistical analysis of flattop distribution fits (FWHM, rise and fall time) to the measured profiles yields the number given in the plot.

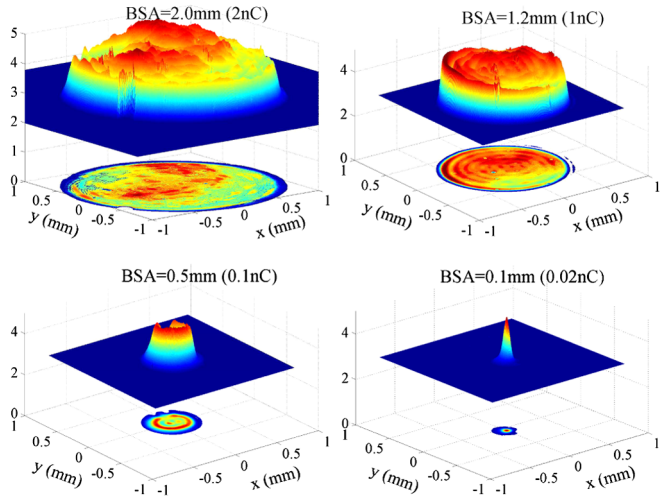

FIG. 6. Typical transverse distributions of the cathode laser for BSAs delivering optimum emittance values for given bunch charges. Laser intensity in arbitrary units is plotted on the vertical axis.

at the location of the BSA, which are originated very probably from contributions of several transverse laser modes as well as from local damages of the conversion crystals. Investigations on the structures of the laser spots for smaller BSAs revealed problems with apertures in the laser beam line. Some optical elements of the imaging and laser beam transport system (like lenses, mirror, and a beam splitter) were placed in the vicinity of the Fourier plane of the BSA to photocathode imaging system and their apertures (as large as 2 inch) were truncating high frequency spatial harmonics. This resulted in radial modulations and deviation from the designed radial flattop shape. These perturbations were most pronounced for smaller spot sizes when the image in the Fourier plane has rather large dimensions. Currently these optical elements are exchanged by 3 to 4 inch components which should improve the imaging.

D. Electron beam diagnostics used in analysis procedure

The transverse emittance of the electron beam is measured downstream of the booster at a distance of 5.74 m from the photocathode using the slit-scan technique [4,5]. The emittance measurement system (EMSY) contains horizontal and vertical actuators supplied with YAG powder (5 μm grain size) and optical transition radiation screens as well as with slit masks made of 1 mm thick tungsten. The slit mask converts a space charge dominated electron beam into an emittance dominated beamlet which is characterized with a screen 2.64 m downstream of the slit. The part of the beam which is hitting the mask is scattered and builds a homogeneous background. By moving the slit mask transversely over the beam spot, one obtains local divergence profiles of the electron beam. The transverse phase space (x, x') can be reconstructed from the whole set of slit-scan data. A YAG screen at the EMSY position is used to measure the rms size of the whole beam σ_x. This value is typically larger than the rms size of the phase space distribution obtained from the slit scan $\sqrt{\langle x^2 \rangle}$. With the assumption that the rms divergence after removing the linear covariance $\langle xx' \rangle$ from the measured phase space is close to the real uncorrelated divergence, the expression for the rms normalized emittance takes the form [5]

$$\varepsilon_{n,x} = \beta\gamma \frac{\sigma_x}{\sqrt{\langle x^2 \rangle}} \varepsilon_{\mathrm{geom},x}, \tag{1}$$

where $\varepsilon_{\mathrm{geom},x}$ is the geometrical emittance and the factor $\beta\gamma = \sqrt{\gamma^2 - 1}$ can be calculated from the relativistic Lorentz factor γ. The electron longitudinal momentum is measured by making use of a spectrometer dipole magnet and a corresponding screen in the dispersive section (DISP2 in Fig. 1). The geometrical emittance $\varepsilon_{\mathrm{geom},x}$ is calculated as

$$\varepsilon_{\mathrm{geom},x} = \sqrt{\langle x^2 \rangle \langle x'^2 \rangle - \langle xx' \rangle^2}. \tag{2}$$

Equations (1) and (2) define the 100% rms normalized projected emittance used at PITZ. More details on the emittance measurement procedure at PITZ can be found in [5].

The bunch charge is measured using integrating current transformers for a range of 0.2–2 nC, lower charges (0.02–0.1 nC) were detected using the Faraday cup in the first diagnostic cross ($\sim$0.8 m from the cathode plane).

III. BEAM DYNAMICS SIMULATIONS

A series of beam dynamics simulations with the ASTRA [12] code were conducted to optimize the PITZ parameter setups for various bunch charges and to support the experimental procedure of the photoinjector optimization. A flattop temporal profile of the cathode laser pulse with 21.5 ps FWHM and 2 ps rise and fall time (close to the measured profiles—Fig. 5) was used in the simulations. A transverse homogeneous laser intensity distribution with variable diameter was applied at the photocathode. Besides the laser spot size, the following parameters were tuned: main solenoid peak field, rf gun launch phase, and the booster gradient. The peak rf electric field at the cathode was fixed at 60.58 MV/m to fit the maximum simulated momentum of the electron beam to the measured one. In order to keep the simulations close to the real conditions the booster peak electric field was restricted to be less than 20 MV/m. All the simulations except dedicated booster phase scans were performed for a booster phase setting allowing maximum acceleration which is reproducing the experimental conditions. A theoretical initial kinetic energy of 0.55 eV was used to simulate a thermal emittance contribution by photoemission from the Cs_2Te cathode [13]. The normalized transverse projected emittance of the electron beam at the EMSY1 location ($z = 5.74$ m) was minimized by tuning the above-mentioned parameters. The simulation results for various bunch charges are summarized in Table I.

The evolution of the transverse projected emittance along the PITZ beam line is shown in Fig. 7 for various bunch charges. The simulated transverse phase space optimized for three bunch charges is shown in Fig. 8.

The dependence of the emittance on the tuning parameters was studied in order to establish the experimental optimization procedure. The emittance growth due to detuning of the solenoid peak field and changing the laser rms spot size at the cathode is shown in Fig. 9. The strong dependence of the projected emittance on the solenoid peak field (10% emittance growth for 0.5% solenoid detuning) makes the solenoid current tuning the major optimization step. The emittance minimum is expected around a main solenoid current of 400 A, therefore a step of 1–2 A is typical for the tuning procedure. As it follows from the simulations, the emittance dependence for low charges (e.g. 0.02 nC) is more relaxed. The emittance dependence

TABLE I. Optimum simulated photoinjector parameters for various bunch charges.

Parameter	Unit	#1	#2	#3	#4	#5
Photoinjector optimized parameters						
Laser σ_{xy}^{l} [a]	mm	0.037	0.102	0.230	0.401	0.600
Gun phase[b]	deg	2.13	1.94	1.81	0.20	−0.83
$E_{z,\mathrm{booster}}^{\mathrm{max}}$ [c]	MV/m	20.0	20.0	20.0	19.76	20.0
$B_{z,\mathrm{solenoid}}^{\mathrm{peak}}$ [d]	mT	224.3	227.0	227.2	227.9	228.4
Electron beam at EMSY1 location, $z = 5.74$ m						
Charge, Q	nC	0.02	0.1	0.25	1.0	2.0
Energy	MeV	23.6	23.6	23.6	23.41	23.6
σ_z [e]	mm	1.74	1.85	1.86	2.16	2.31
$\varepsilon_x^{\mathrm{projected}}$	mm mrad	0.061	0.173	0.262	0.607	1.144
$\langle\varepsilon_x^{\mathrm{slice}}\rangle$ [f]	mm mrad	0.044	0.121	0.219	0.538	0.978

[a]Root-mean square (rms) size of the round laser spot $\sigma_{xy}^{l} = \sqrt{\sigma_x^l \sigma_y^l} = \sigma_x^l = \sigma_y^l$.
[b]With respect to the phase of the maximum mean momentum gain (MMMG).
[c]The peak electric field in the CDS booster is restricted; if the optimization goes above 20 MV/m it was automatically set to this threshold.
[d]Peak field of the main solenoid. The bucking solenoid was always tuned to compensate the longitudinal magnetic field at the cathode.
[e]The rms bunch length.
[f]The averaged slice emittance within the bunch.

on the rms size of the laser spot at the cathode has a steeper slope for smaller sizes due to the space charge induced dilution of the phase space. Increasing laser spot sizes w.r.t. the optimum value leads to a growth of the uncorrelated emittance due to the thermal emittance contribution. Typically 10%–20% rms spot size detuning resulted in 10% simulated emittance growth. This implies that a ~50 μm step in the laser spot diameter has to be used. This was considered for the production of a BSA plate with diaphragm diameters smaller than 0.7 mm (see Sec. II C).

The emittance sensitivity to phase variations is illustrated in Fig. 10 (left plot). The dependence of the emittance on the rf gun launch phase (10% growth for ±2 deg phase detuning) determines a step of 2–3 deg for the gun

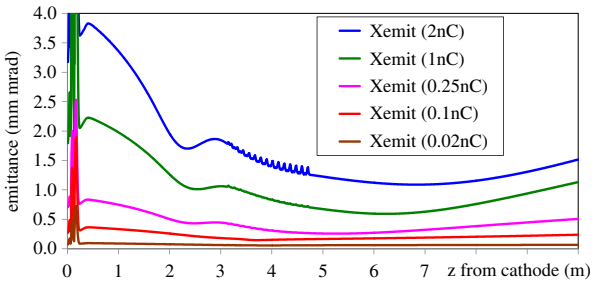

FIG. 7. Normalized transverse projected emittance along the PITZ beam line for various bunch charges. Optimum photoinjector setups from Table I were used.

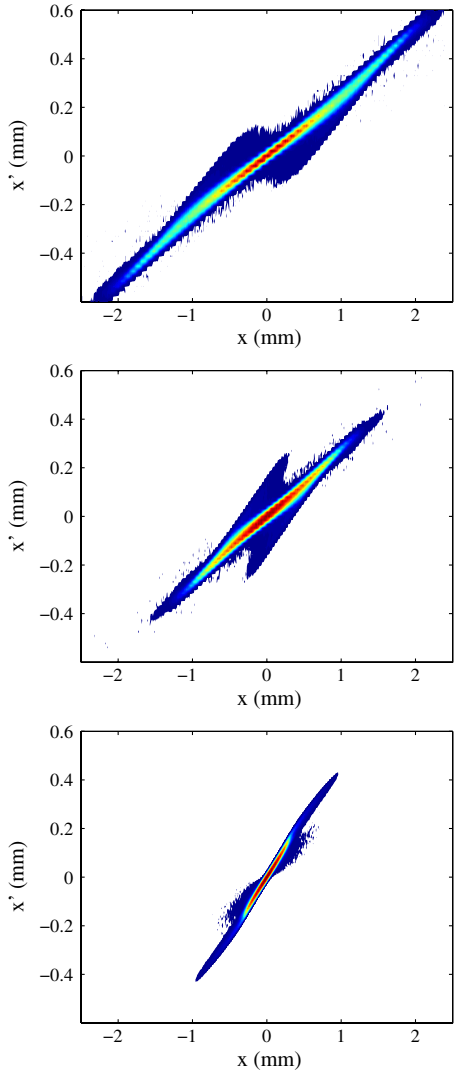

FIG. 8. Simulated transverse phase space at the location of EMSY1 for 2 nC (upper plot), 1 nC (middle plot), and 0.1 nC (bottom plot).

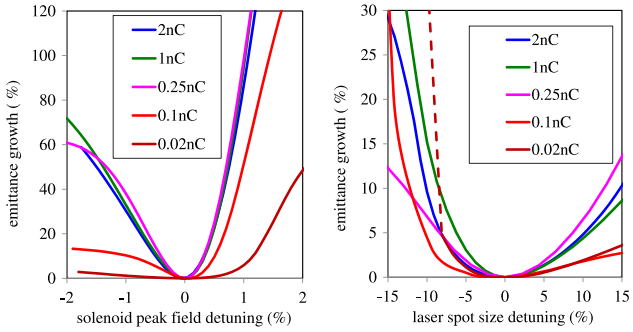

FIG. 9. Simulated emittance growth as a function of the solenoid peak field detuning $B_{z,\mathrm{solenoid}}^{\mathrm{peak}}/B_{z,\mathrm{solenoid}}^{\mathrm{peak,optimum}} - 1$ (left plot) and as a function of the laser spot size detuning $\sigma_{xy}^{l}/\sigma_{xy}^{l,\mathrm{optimum}} - 1$ (right plot). The part of the curve for 0.02 nC shown with a dashed line corresponds to the case of the space charge limited emission when the desired bunch charge cannot be extracted from the cathode.

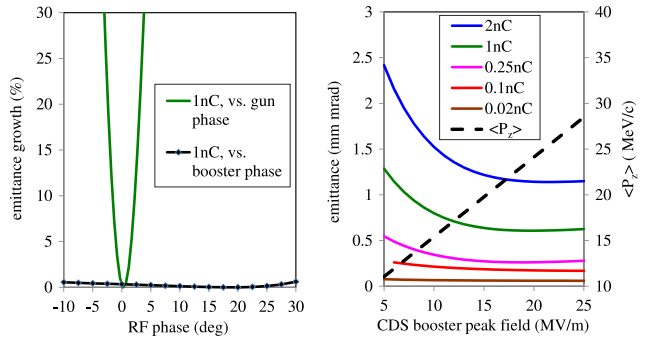

FIG. 10. Simulated emittance growth as a function of the rf phase of the gun and the booster (left plot). Both phases are calculated w.r.t. the phase of the maximum mean momentum gain. Right plot—simulated emittance as a function of the booster peak field. The final mean momentum of the electron beam is plotted at the right axis.

phase tuning. Although the dependence of the rms emittance value on the gun rf phase is rather weak, the experimental dependence is expected to be much stronger due to the fact that the phase space correlation is strongly dependent on the gun phase. It means that even a small slope of the gun phase within the bunch pulse train leads to the overlapping of phase spaces for different gun phases resulting in a significant increase of the measured emittance [5]. Shot-to-shot phase noise causes an additional increase of the measured projected phase space area.

The simulated emittance dependence on the booster phase is much weaker. A linear emittance growth rate of $0.02\%/$ deg was obtained at the MMMG booster phase. A very shallow emittance minimum was simulated for the booster phase of ~ 20 deg off-crest, the relative emittance increase at the MMMG phase is only 0.35%. But significant energy spread of the electron beam makes the formally obtained optimum booster phase of no practical use, because the measured transverse phase space could be spoiled by large momentum spread of the electron beam. That is why for simulations as well as for experimental optimization the booster phase for the maximum acceleration has been used.

Simulated emittance as a function of the peak field in the CDS booster is plotted at the right plot in Fig. 10. The optimum field strength was found to be about 20 MV/m resulting in a final beam momentum of 24 MeV/c which is close to the experimental conditions of the booster operation at maximum available rf peak power. Bigger emittance values at lower booster gradients simulated for higher bunch charges (2 and 1 nC) are results of the space charge effect which is more significant for these charges at lower beam energies. So far, the laser pulse length as well as the booster position in the linac were kept fixed for these simulations, resulting in rather weak dependencies of the emittance on the booster gradient for low charges.

IV. EMITTANCE EXPERIMENTAL OPTIMIZATION

A. Optimization procedure

The experimental procedure for minimizing the projected normalized emittance for a given bunch charge consists of a set of consequent steps.

1. Laser temporal profile.—The temporal profile of the cathode laser pulse is checked using the OSS. The goal shape is a zero-sloped flattop distribution with shortest possible rise and fall time and smallest intensity modulations. By tuning of corresponding crystals in the pulse shaper it was possible to keep the flattop profile with ~ 21.2 ps FWHM and ~ 2.3 ps rise/fall time (see Fig. 5).

2. Laser transverse distribution.—A BSA is inserted to produce the desired laser spot size on the cathode. The laser transverse distribution is monitored by a UV sensitive CCD camera. The radial homogeneous distribution serves as a goal for the transverse laser profile. The optimization was realized by transverse displacement of the BSA to the position within the incident laser beam with highest integral homogeneity. This is followed by the beam based alignment of the laser on the photocathode [14].

3. RF gun phase.—The rf gun phase is adjusted w.r.t. the phase of the maximum mean momentum gain (MMMG). The momentum measurements in the low energy dispersive arm as a function of the gun launch phase are done using 1 deg step with already tuned rf feedback in the gun cavity. Because of flatness of the mean momentum dependence on the gun phase, the MMMG phase was defined with an accuracy of ~ 0.5–1 deg. Then an offset from the MMMG phase is set and the momentum distribution is measured for this working phase (i.e. for the gun phase to be used for the emittance measurements). A step of 3 deg has typically been used for the emittance optimization as a function of the gun phase. The laser intensity fine-tuning to produce a given bunch charge for the adjusted gun phase is completing this step of the optimization procedure.

4. Booster phase.—The booster phase is adjusted w.r.t. the MMMG phase. The booster gradient (rf power in the cavity) was typically tuned to the maximum available value according to expectations from beam dynamics simulations (see Fig. 10). The beam momentum measurements in the high energy dispersive arm as a function of the booster phase are used to find the booster MMMG phase. It should be noticed that the rf pulse duration in the gun and in the booster is adjusted to support the electron bunch train length needed for emittance measurements, typically 300 μs long rf pulses were used.

5. Emittance measurements versus main solenoid current.—Emittance measurements as a function of the main solenoid current are performed. Geometrical emittance [see Eq. (2)] is measured using a slit-scan technique which consists of several steps.

(i) The electron beam transverse distribution is measured at the EMSY screen, i.e., at the z location of the

slit masks. The main output of this step are rms beam sizes σ_x and σ_y used in Eq. (1). Typically 10 frames with a beam image are taken for statistics, 10 frames with background (laser shutter closed) are used to clean the image from the noise originating from dark current and from electronic noise of the TV system. The typical rms error of the beam size measurements is less than 1%. In order to use the dynamic range of the 12-bit camera as much as possible the maximum intensity of the beam image is adjusted to have pixels with values of at least ~3000 but still not to be saturated (the saturation level is $2^{12} - 1 = 4095$). This intensity criterion ("3000-criterion") is achieved by interplay of the camera gain and the number of pulses in a train, while keeping the number of pulses as low as possible to minimize the influence of the beam jitter.

(ii) An image of the whole beam is also taken at the beamlet collector screen (downstream of the EMSY). The same intensity criterion is used for the image taking. This image is converted into a binary function in order to produce the mask of interest (MOI), within which beamlets will be considered. All signals outside the MOI are to be discarded.

(iii) A slit scan to measure the local divergence profile is synchronized with beamlet image taking at the collector screen. A typical speed of the slit mask movement is 0.5 mm/s whereas the images are taken at an average rate of 10 Hz, i.e., the separation of the slit images is ~50 μm. The intensity criterion described above is now applied to the set of all beamlet images. After image processing each beamlet profile can be associated with a slit position inside the beam. This allows a phase space reconstruction.

The main solenoid current is set through the maximum value (500 A) in order to prevent the hysteresis ambiguity, so the solenoid scan is performed from higher to lower values in the scan range. The bucking solenoid is tuned each time to compensate the longitudinal magnetic field at the cathode; for the solenoid correlation the following formula is applied in the control system $I_{\mathrm{buck}}[A] = 0.0673 + 0.0827 \cdot I_{\mathrm{main}}[A]$. A typical step of 1–2 A is used for this scan. For each solenoid current both x and y emittances are being consequently measured.

6. Statistical measurements for the best point.—For the solenoid current I^*_{main} delivering the smallest value of the geometrical mean $\sqrt{\varepsilon_{n,x} \cdot \varepsilon_{n,y}}$, $N \times M$ statistical measurements of emittance are taken. This implies N series of emittance measurements [items (i) and (ii) in Sec. IV A 5], with the slit scans [item (iii) in Sec. IV A 5] for each series repeated M times. This reproducibility check has the goal to control the stability of the obtained emittance minimum.

B. Emittance improvements from 2009 to 2011

As mentioned in Sec. II, several significant improvements were implemented at PITZ for the 2011 running compared to the 2009 run period. These modifications, namely, a feedback for the gun rf power regulation using a 10-MW in-vacuum directional coupler, a new CDS booster with longer acceleration length, higher available booster gradients and capability to run with longer rf pulses, some modifications in the laser transport beam line, and several improvements in the electron beam line, resulted in better machine performance. In order to evaluate this improvement the beam emittance has been reoptimized for the same charges as in 2009 [5]. A comparison of the results is shown in Fig. 11, where emittance values measured in 2011 (solid curves) are shown as a function of the laser rms spot size at the cathode for 3 different charges compared to corresponding measurements from 2009 (dashed lines).

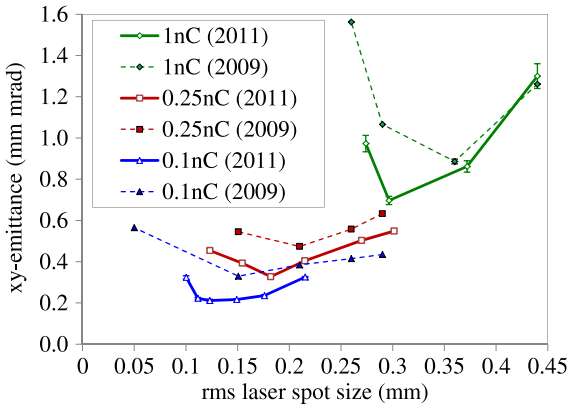

FIG. 11. Measured rms normalized emittance as a function of the rms laser spot size at the cathode. For comparison the results of the optimization in 2009 are plotted with dashed lines. The statistical error bars (see Sec. IV A 6) are included in the graph but small statistical error bars are hidden behind markers in the plot.

The experimental emittance optimization has revealed that the above mentioned upgrade resulted in a significant reduction of the measured emittance minima. The minimum geometrical mean emittance values obtained in 2011 for various bunch charges are summarized in Table II. The relative emittance reduction is larger for smaller charges, which is definitely an effect of the implementation of the low level rf regulation of the gun phase. In order to fulfill the intensity criterion of the beam measurements (described in IV A) longer pulse trains have to be used for lower charges. Therefore the significantly improved rf

TABLE II. Minimum emittance measured in 2011 $\varepsilon_{xy}(2011)$ and corresponding emittance reduction since 2009 $\delta\varepsilon = \varepsilon_{xy}(2011) - \varepsilon_{xy}(2009)$.

Bunch charge	$\varepsilon_{xy}(2011)$	$\delta\varepsilon/\varepsilon_{xy}(2009)$
1.0 nC	0.696 ± 0.020 mm mrad	−21%
0.25 nC	0.328 ± 0.010 mm mrad	−31%
0.1 nC	0.212 ± 0.006 mm mrad	−36%

gun phase stability (Fig. 3) and the minimum phase slope within the pulse train have a larger impact on low charge measurements. Besides this, a more stable phase resulted in smaller electron beam positioning jitter at EMSY1. Because of smaller electron beam sizes for smaller bunch charges, the improved phase stability is stronger affecting the measured emittance for lower charges. The same explanation is also valid for another important observation from the comparison in Fig. 11—a reduction of the optimum rms spot size of the cathode laser. Although the same BSA set has been used for the 1 nC optimization in both run periods, the BSA delivering the minimum emittance is smaller in 2011 compared to the 2009 run period. This small shift in rms sizes of the laser spot can be explained by the above-mentioned improvements in the laser transport beam line yielding a better homogeneity of the transverse distribution. The increased number of BSA's available in 2011 gave the ability of finer scans especially for low bunch charge (Fig. 11). It should be noticed that each data point in Fig. 11 is a result of a main solenoid current optimization. Furthermore, for the case of 1 nC an rf gun phase optimization had also been performed.

C. Emittance versus bunch charge

Besides bunch charges of 1, 0.25, and 0.1 nC two additional charges were newly optimized for minimum emittance: 2 and 0.02 nC. The measured projected xy emittance (geometric mean of the values for the x and y plane $\sqrt{\varepsilon_{n,x} \cdot \varepsilon_{n,y}}$) as a function of the laser rms size at the cathode is shown in Fig. 12 for the various bunch charges together with simulated curves. All simulated curves are obtained from laser spot size variation around the optimum value while the other machine parameters were fixed to

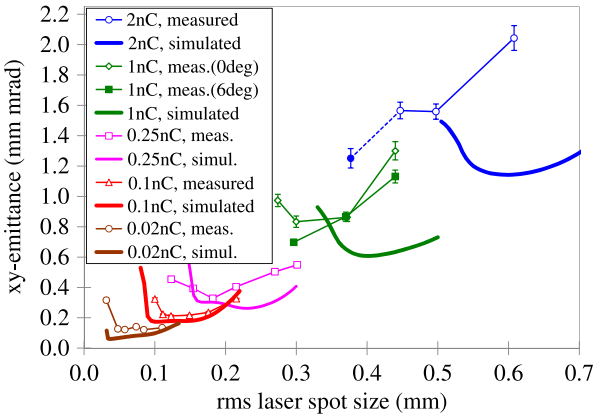

FIG. 12. Measured and simulated rms normalized emittance as a function of the laser spot size at the cathode for various bunch charges. The two experimental curves for 1 nC correspond to different gun phases. Empty markers of the 2 nC curve indicate gun operation at MMMG phase, whereas the filled marker shows the emittance value measured for +6 deg gun phase. As before the statistical error bars corresponding to Sec. IV A 6 are shown.

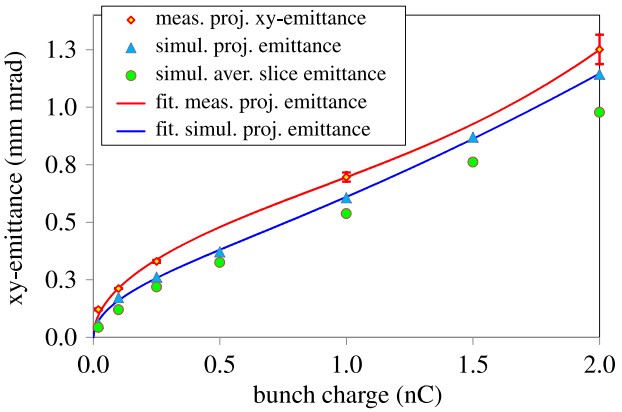

FIG. 13. Measured rms normalized emittance as a function of bunch charge. The blue and the green markers present the results of the beam dynamics simulations for various charges from Table I. The red and blue curves for the measured and simulated projected emittance were obtained using the formula $\varepsilon_{\text{fit}} = \sqrt{a \cdot q + b \cdot q^c}$ (see text for more details).

values given in Table I. One can clearly see a rather large discrepancy in the optimum laser spot size for higher bunch charges (2, 1, and 0.25 nC); this discrepancy becomes smaller with decreasing charge resulting in a quite good agreement for 0.1 nC. The possible reason of this discrepancy will be discussed later (Sec. IV E).

The summary of the minimum measured projected emittance (geometrical mean values) as a function of bunch charge q is shown in Fig. 13 together with the simulated projected emittance. The simulated averaged slice emittance is shown as well in order to illustrate the quality of the emittance optimization.

Several parameters were optimized in the experiment as well as in beam dynamics simulations: laser spot size at the cathode, rf gun launch phase and main solenoid peak field, while the temporal laser profile was fixed. This corresponds to different contributions from the space charge, rf, and chromatic effects to the emittance budget for various bunch charges. For cases of lower charge the electron beam shape is closer to the model of a long beam ($\sigma_z \gg \sigma_{x,y}$) and the relative space charge contribution to the emittance is smaller than in cases of higher charge, when the transverse and longitudinal dimensions of the electron beam are comparable. The dependence of the optimum laser spot size at the cathode on the bunch charge can reasonably be approximated with a square root law. This means that also the thermal emittance which is linearly dependent on the laser spot size is expected to have a square root dependence on the bunch charge. An estimation on the charge scaling for the space charge derived emittance $\varepsilon^{\text{sc}} \sim q^{2/3}$ can be obtained from the envelope equation [15] where all three bunch dimensions are equally scaled keeping the bunch aspect ratio constant. The same approach to the rf and chromatic contributions to the emittance results in a charge dependence as $\sim q^{4/3}$ [16].

But this equal bunch dimensions scaling does not take place for the experimental conditions described in this work, where the cathode laser pulse duration was fixed for all optimized bunch charges. According to beam dynamics simulations, the bunch aspect ratio is varied by more than a factor of 3 for the bunch charge range between 0.02 and 2 nC, whereas the electron bunch length increase (due to the longitudinal space charge) is ~30% (Table I). This implies that the space charge effect is significantly modified for various bunch charges which makes modeling of the charge scaling rather complicated. Applying the formula $\varepsilon_{\mathrm{fit}} = \sqrt{a \cdot q + b \cdot q^c}$ to fit the measured and the simulated emittance, one can try to separate the thermal emittance (the first term under the square root corresponds to the thermal emittance squared) from other contributing factors (the second term). Such a fit procedure applied to the simulated emittance results in $\varepsilon_{\mathrm{fit}}^{\mathrm{sim}} = \sqrt{0.255 \cdot q + 0.117 \cdot q^{2.7758}}$ (the blue curve in Fig. 13). A corresponding fit to the measured projected emittance yields $\varepsilon_{\mathrm{fit}}^{\mathrm{meas}} = \sqrt{0.457 \cdot q + 0.028 \cdot q^{4.56}}$ (the red curve in Fig. 13). According to the obtained fits the growth rate of the space charge impact for high charge onto the measured emittance is significantly stronger than for the simulated emittance. Another interesting conclusion from these fits concerns the thermal emittance contribution. Comparing the coefficients for simulated and measured projected emittance and taking into account the photoelectron kinetic energy of $E_k = 0.55$ eV used in the simulations, a rough estimation of the experimental E_k value yields 0.74 eV.

D. Emittance versus main solenoid current

The basic measurement of the emittance optimization is to measure an rms normalized emittance in both planes as a function of the main solenoid current. Typical measured emittance curves as a function of the main solenoid current are shown in Fig. 14 for various bunch charges. Dashed curves for 1 and 2 nC correspond to the gun operation at +6 deg w.r.t. the MMMG phase.

It should also be noted that the curves for 2 nC were obtained for different laser rms spot sizes at the cathode (0.5 mm for 0 deg gun phase and 0.38 mm for +6 deg) whereas both curves for the 1 nC case were measured for 0.3 mm laser rms spot size. It can be seen clearly that the optimum current of the main solenoid is higher for +6 deg (by 1 A for 2 nC and by 4 A for 1 nC) compared to the zero phase curves. The optimum point shift to higher solenoid currents (thereby stronger focusing strength) can be explained by the higher accelerating field at the cathode at the moment of emission for a positive phase offset from the MMMG phase.

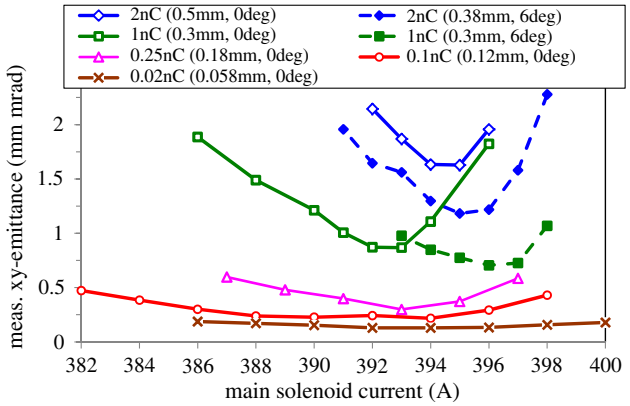

FIG. 14. Measured rms normalized xy emittance as a function of the main solenoid current. Curves for the optimum rms size of the cathode laser spot (size parameter in the legend) are shown. For bunch charges of 1 and 2 nC two gun phases—0 deg and 6 deg w.r.t. MMMG phase—are included, whereas for other charges the gun was operated at MMMG phase.

E. Emittance versus rf phase

It has been found experimentally that the rf gun launch phase has a more significant impact onto the measured beam projected emittance than it was expected from beam dynamics simulations (Fig. 10). Moreover, the experimental optimum phase for higher bunch charges (1 and 2 nC) is about +6 deg whereas the simulations deliver the smallest emittance even at small negative offset from the MMMG phase (Table I).

Dependences of the measured bunch charge on the rf gun launch phase (so-called phase scans) are shown in Fig. 15. A maximum mean momentum of ~6.7 MeV/c was measured; the momentum scan curve around the MMMG phase is shown as well. An estimation of the rf electric field at the cathode (black solid curve in Fig. 15) yields about an 8% field increase at +6 deg gun phase

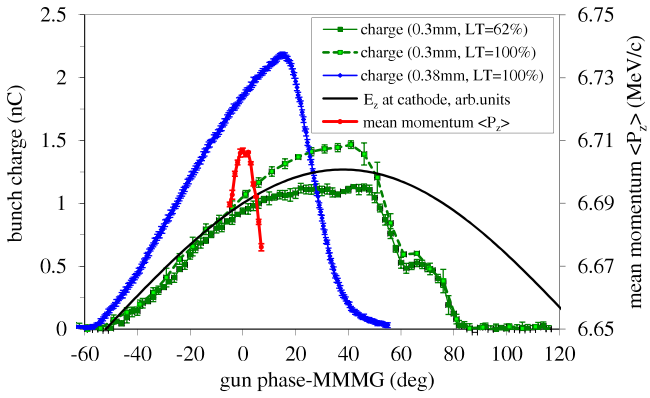

FIG. 15. Measured charge as a function of the gun phase w.r.t. the MMMG phase. Different curves correspond to various rms spot sizes of the laser at the cathode (0.3 and 0.38 mm) and different laser intensities (laser transmission—LT). The measured mean momentum after the gun is plotted against the right axis. The longitudinal component of the rf electric field at the cathode is plotted against the left axis. This curve is normalized to the field at the MMMG phase.

compared to zero phase. A phase of −52 deg w.r.t. MMMG phase was assumed to correspond to a zero crossing of the rf field at the cathode.

The shape of these phase scans corresponds to the strong influence of space charge and Schottky-like effects (particle emission enhancement in the presence of strong electric fields) on charge production. The blue and green solid curves correspond to the case of optimum measured emittance (gun phase of +6 deg). Direct plug-in of experimental parameters into ASTRA does not yield the expected bunch charge due to space charge limited emission, whereas a bunch charge of 1 and 2 nC has been detected in experiment. In the case of a 0.38 mm laser spot size at the cathode (blue curve in Fig. 15), it was not possible to produce 2 nC at the MMMG phase but only at +6 deg. For the laser rms spot size of 0.3 mm a bunch charge of 1 nC was attainable for both phases.

The space charge effect at the photocathode has also impact onto the longitudinal phase space (LPS) of the emitted bunch. Unfortunately, due to technical problems no direct LPS measurements were available in 2011, only longitudinal momentum distribution measurements were routinely performed during machine setup for the emittance measurements. The mean momentum and the rms momentum spread measured in the low energy dispersive section (DISP1 in Fig. 1) as a function of the rf gun phase is shown in Fig. 16 (upper plot). To simulate these dependencies two laser spot sizes were used: $\sigma_{xy}^{l} = 0.32$ mm [the first simulation setup—"simul. (1)"] and $\sigma_{xy}^{l} = 0.40$ mm [the second simulation setup—"simul. (2)"—which is close to the optimum simulated emittance case]. The rf longitudinal electric field at the cathode was tuned to ∼60.9 MV/m in the simulations in order to fit the measured mean momentum $\langle P_z \rangle$. Other simulation settings were chosen to be close to the experimental machine parameters. The first simulation setup corresponds to a strongly space charge affected emission; charge losses of ∼30 pC from the initial 1 nC were simulated for the MMMG gun phase. Because of a larger laser spot size at the photocathode the charge extraction for the second simulation setup was smooth, the whole 1 nC bunch charge was accelerated. The lower plot in Fig. 16 shows the mean momentum and rms momentum spread measured in the first high energy dispersive section (DISP2 in Fig. 1) as a function of the booster rf phase. The corresponding simulated curves applying the above-mentioned two setups are also shown in the plot. The gun phase was tuned to be +6 deg w.r.t. MMMG phase during measurements as well as for both cases of simulations. The simulations were performed until the entrance of the dipole magnets, whereas the measured momentum distributions are affected by a finite transverse beam size in the dispersive section. This effect can be responsible for the discrepancy between measured and simulated rms longitudinal momentum spread. Nevertheless, the fact that both simulation setups yield longitudinal momentum distributions close to the measured ones provides a comparability of experimental and simulated longitudinal phase space. This gives an estimation of the rms bunch length—2.6 mm for the "simul. (1)" setup and 2.2 mm for the "simul. (2)".

The dependence of the measured emittance on the gun phase has been studied for the case of 1 nC bunch charge—the summary of measured xy emittances is shown in Fig. 17. The booster gradient and phase were tuned for

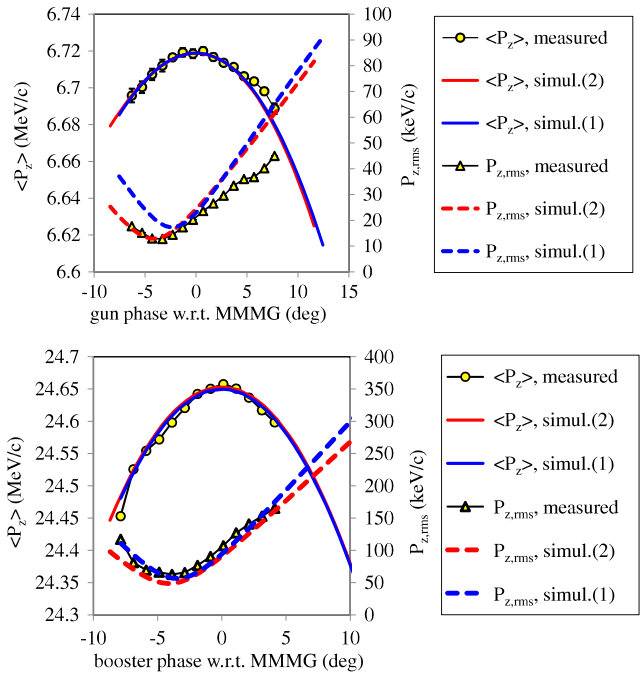

FIG. 16. Measured and simulated mean momentum and rms momentum spread as a function of gun (upper plot) and booster (bottom plot) phase. Results of two simulation setups are shown corresponding laser rms spot size at the phototcathode: "simul. (1)", with $\sigma_{xy}^{l} = 0.32$ mm, and "simul. (2)", with $\sigma_{xy}^{l} = 0.4$ mm.

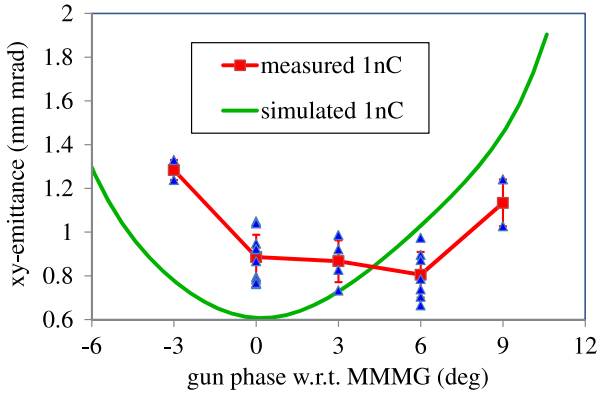

FIG. 17. Measured and simulated 1 nC emittance as a function of the gun phase w.r.t. MMMG phase. The measurements have been performed using an rms laser spot size of 0.3 mm. Parameters corresponding to Table I were applied for the simulations.

these studies to the maximum available momentum gain resulting in a final beam mean momentum of ~25 MeV/c. The laser rms spot size was fixed at 0.3 mm. Each point in Fig. 17 corresponds to the minimum xy emittance value obtained from a corresponding scan of the main solenoid current.

The simulated dependence of the emittance on the gun phase is shown in Fig. 17 as well. The simulated optimum phase of 0.2 deg has a rather large offset from the experimentally obtained optimum value (+6 deg). This can be (at least partially) explained by the experimental optimum laser spot size at the cathode which is about 25% smaller than the simulated one. This implies that the experimental space charge density at the cathode is 1.8 times higher than in the simulations, requiring a phase shift towards higher emission fields.

F. Emittance versus booster gradient

Several studies of the emittance dependence on the booster gradient have been performed before the final optimization for 1 nC bunch charge took place. The projected emittance was measured for a laser rms spot size of 0.3 mm. The gun was operated at the maximum mean momentum gain gradient and phase. For each booster gradient the booster phase was tuned to yield the maximum mean momentum of the electron beam. The measured and simulated xy emittance as a function of the final beam momentum is shown in Fig. 18. For the simulated curve the booster gradient was varied for the optimum parameters of a 1 nC beam (Table I). Measurements and simulations show the same trend with an offset. Further experiments will be conducted.

G. Detailed emittance studies for 1 nC

Since 1 nC remains one of the nominal bunch charges for the European XFEL, a major part of the operation time at PITZ in 2011 was devoted to the detailed emittance optimization at this charge level. A summary of the optimized emittance for 1 nC is illustrated in Fig. 19, where the best values of the geometrical mean of both transverse planes obtained from the experimental optimization are plotted for three gun phases.

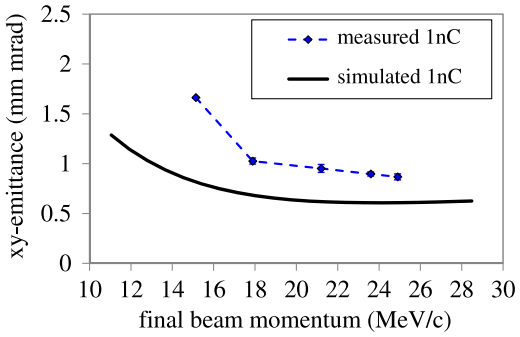

FIG. 18. Measured and simulated emittance as a function of the beam momentum after the booster. The final beam momentum was adjusted only by variation of the booster gradient. The rf phases of gun and booster were always tuned to MMMG phase for the experimental results.

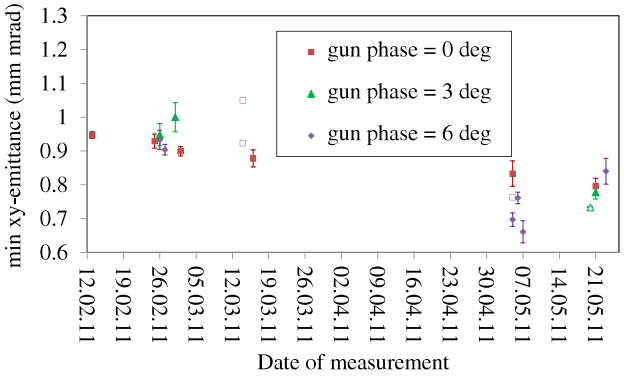

FIG. 19. Measured emittance versus date of measurement for different gun phases w.r.t. the MMMG phase. Solid markers correspond to the results from statistics measurements (see Sec. IV A 6) whereas empty markers depict minimum values directly from solenoid scans (see Sec. IV A 5).

Several steps in the machine improvement were undertaken in April 2011. The most significant were changes in the optical transport beam line for the cathode laser resulting in a more homogeneous transverse distribution and removing of magnetizable components from the electron beam line to reduce their influence, especially in the low energy section. This resulted in a significant reduction of the measured emittance in May (see Fig. 19).

The systematic uncertainty of the measurement is in general larger than the statistical error. The largest contribution to the systematic error is the nonperfect reproducibility of the measurement conditions at different days, e.g., due to small drift in the transverse and longitudinal cathode laser profiles, different tuning of the low level rf feedback loop and water regulation due to different rf

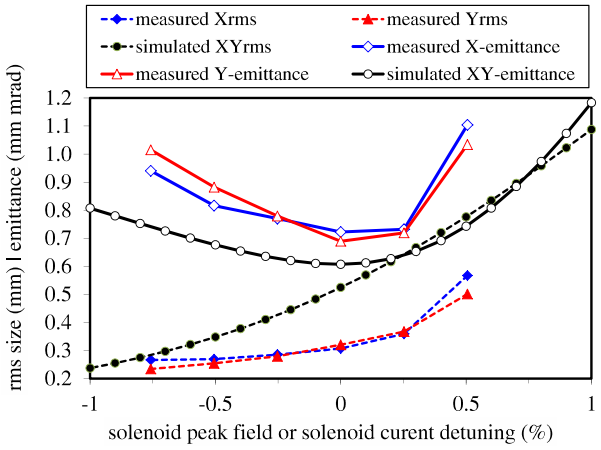

FIG. 20. Measured and simulated rms size and emittance at EMSY1 for 1 nC versus main solenoid current detuning.

parameters, slow cathode degradation, modified trajectory of the electron beam through the accelerator, and so on. A measure of the total size of such systematic uncertainties can be estimated from the measurements for 1 nC performed in May 2011 (see Fig. 19) when the lowest emittance values were obtained. The rms width of the emittance results in this time period is $\Delta_{\mathrm{sys}} = 0.079$ mm mrad, or $\sim$11% of the mean value, whereas the averaged statistical error is 0.023 mm mrad.

A typical solenoid scan for 1 nC (measured horizontal and vertical rms beam size and emittance) is shown in Fig. 20 as a function for the main solenoid detuning $I_{\mathrm{main}}/I^{*}_{\mathrm{main}} - 1$, where $I^{*}_{\mathrm{main}} = 396$ A is the solenoid current of the minimum xy emittance. Corresponding simulated curves (Table I) are also shown as a function of the solenoid peak field detuning. The final reproducibility check (statistics) for $I^{*}_{\mathrm{main}} = 396$ A resulted in $\varepsilon_{n,x} = 0.707 \pm 0.032$ mm mrad and $\varepsilon_{n,y} = 0.686 \pm 0.024$ mm mrad, which corresponds to a geometrical mean value of $\varepsilon_{n,xy} = 0.696 \pm 0.020$ mm mrad.

The fact that the measured emittance values are higher than those expected from the beam dynamics simulations can be explained by imperfections of the machine and measurement procedure. In contrary, why the measured rms size of the electron beam is significantly smaller than the simulated values is not fully understood. It should be noticed that for the optimum simulations for 1 nC the rms spot size of the cathode laser is $\sim$30% larger than those resulting from the experimentally optimized BSA size. This significant difference in the space charge density at the cathode indicates that the discrepancy probably originates from the space charge dominated photoemission. Also the experimentally found rf gun optimum phase of +6 deg corresponds to a higher electric field at the cathode at the emission moment. This can partially explain the smaller optimum laser spot size and higher solenoid currents yielding the emittance minimum. But the corresponding decrease of the thermal uncorrelated emittance contribution due to smaller initial beam size cannot explain the smaller rms size of the electron beam observed at EMSY1.

In order to study the role of the emission area homogeneity, a dedicated test has been performed. After the emittance optimization, the photocathode #110.2 which was actively used in the operation was replaced by a fresh cathode #11.3 [17]. Before and right after the cathode exchange, the QE maps of both cathodes were measured by scanning the cathode surface with a small laser spot ($\sim$ 0.2 mm diameter) with 0.2 mm steps in the x and the y direction. The measured QE maps are shown in Fig. 21 (upper plots). The old cathode has a rather large QE inhomogeneity especially in the center area. This is an indication of an active cathode usage especially for the low charge optimization when small laser spot sizes and long pulse trains were applied. The new cathode on the other hand shows a very homogeneous QE map. Because of the necessity to change the BSA for the QE-map measurements, it was not possible to reproduce the laser transverse distribution (Fig. 21, bottom left plot) after the cathode exchange. Reinsertion of the laser BSA of 1.2 mm diameter resulted in a more homogeneous laser transverse distribution (Fig. 21, bottom right plot). It is hard to separate the effect of the more homogeneous QE map of the fresh cathode from the improved laser transverse distribution but the homogeneity of the emission (which can be presented as a convolution of the QE map and the laser transverse distribution) was significantly improved.

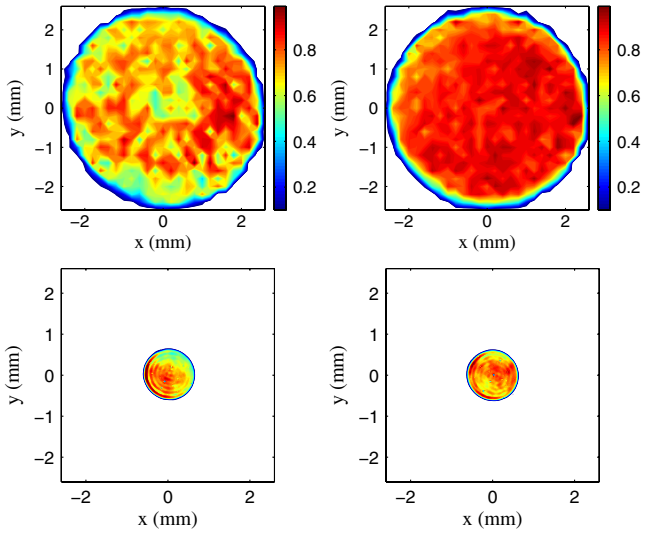

FIG. 21. Upper row: QE maps of the used cathode #110.2 (left) and the fresh cathode #11.3 (right). Bottom row: corresponding transverse laser intensity distributions at these cathodes used for emittance measurements.

The best machine setup (laser rms spot size of $\sim$0.3 mm and gun phase of +6 deg) was applied, the main solenoid current scan for the best emittance was performed for each case, resulting in the optimum solenoid current of 396 A. The results of the emittance optimization for these two different Cs_2Te cathodes performed within one day are summarized in Table III. The corresponding optimum phase space measured before and after the cathode exchange is shown in Fig. 22. Despite rather small visual differences in the measured electron beam distributions, the phase space measured after the cathode exchange is more symmetric, having sharper edges. The observed x-y asymmetry remains but is being modified. It should be

TABLE III. Emittance for a 1 nC beam measured for different cathodes.

Cathode	$\varepsilon_{n,x}$, mm mrad	$\varepsilon_{n,y}$, mm mrad	$\varepsilon_{n,xy}$, mm mrad
#110.2	0.742 ± 0.021	0.782 ± 0.028	0.762 ± 0.017
#11.3	0.724 ± 0.056	0.603 ± 0.038	0.661 ± 0.033

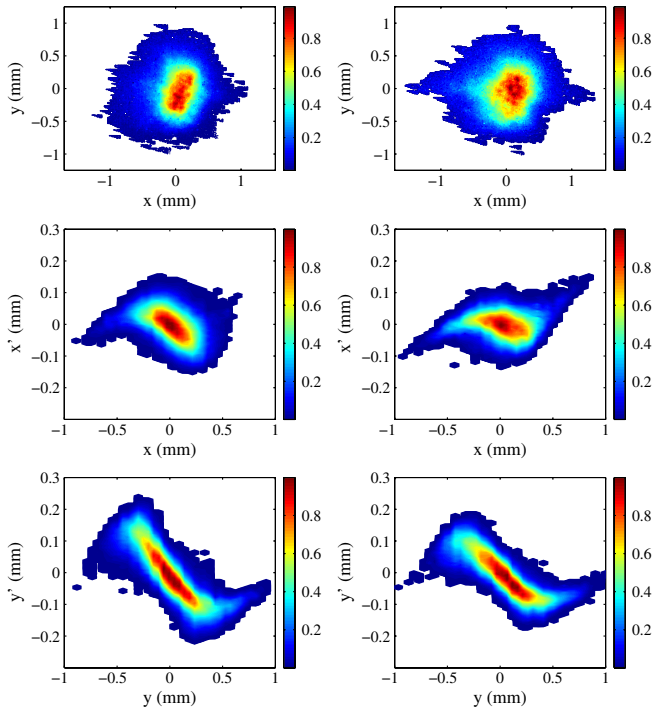

FIG. 22. Measured beam x-y distribution at EMSY1 (upper row), horizontal (middle row), and vertical phase space (bottom row) for a bunch charge of 1 nC. A main solenoid current of 396 A, rf gun phase of +6 deg and laser rms spot size of 0.3 mm were applied. The left column of plots corresponds to the measurements with the cathode #110.2, the right column those with the cathode #11.3 (see Table III).

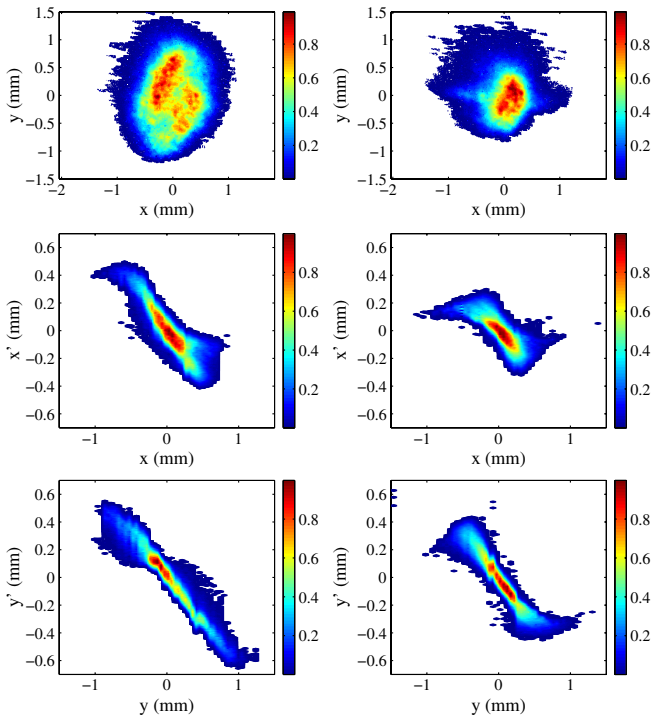

FIG. 23. Measured beam x-y distribution at EMSY1 (upper row), horizontal (middle row), and vertical phase space (bottom row) for a bunch charge of 2 nC. The left column of plots corresponds to the measurements with BSA = 2.0 mm and the main solenoid current of 394 A, the right column of plots is for BSA = 1.5 mm and $I^*_{\mathrm{main}} = 395$ A.

noticed that the measured optimum phase space for 1 nC differs quite significantly from the phase space optimized for the minimum emittance in the simulations (Fig. 8).

H. Emittance optimization for 2 nC

A remarkable feature of linacs based on the TESLA technology is the possibility of high charge operation. The PITZ gun with a Cs_2Te photocathode is capable to produce electron bunches with up to several nC bunch charge. Simulations of SASE processes for the European XFEL assuming high bunch charge (>1 nC) [18] show attractive properties of such a radiation, especially for the peak radiation power.

In order to study high charge operation, the emittance was experimentally optimized for 2 nC bunches. Several laser BSAs (2.5, 2.0, and 1.8 mm diameter) were tested for best emittance while the gun was operated at MMMG phase. For each spot size a solenoid scan was performed to minimize the xy emittance. The best results for the MMMG phase are shown with empty markers in the blue curve in Fig. 12. The best emittance for 2 nC for this gun phase was obtained for the BSA diameter of 2.0 mm (0.50 mm rms spot size) and measured to be $\varepsilon_x = 1.470 \pm 0.081$ mm mrad and $\varepsilon_y = 1.652 \pm 0.056$ mm mrad ($\varepsilon_{xy} = 1.558 \pm 0.050$ mm mrad). The emittance result for the 1.8 mm BSA diameter (0.45 mm rms spot size) was about the same within the experimental error bar. Continuing the scan towards smaller spot sizes was not possible due to availability of BSA's and the limitation by space charge, as discussed in Sec. IV E. By applying a +6 deg phase offset a bunch charge of 2 nC was reached and corresponding emittance optimization was performed. The solenoid scan for this setup resulted in the best emittance value at $I^*_{\mathrm{main}} = 395$ A; the reproducibility check yielded $\varepsilon_x = 1.239 \pm 0.088$ mm mrad and $\varepsilon_y = 1.267 \pm 0.093$ mm mrad ($\varepsilon_{xy} = 1.251 \pm 0.064$ mm mrad). The measured phase space and transverse beam distributions are shown in Fig. 23 for both cases. The phase space nonlinearity is stronger for the case of the smaller laser spot at the cathode which is a definite signature of space charge impact. Another observation is a horizontal structure in the x-y beam distribution which was observed for the case of 1 nC, but is more pronounced for the stronger space charge dominated case of 2 nC and BSA = 1.5 mm. The origin of such a structure is not fully understood; a possible reason could be an impact of the vacuum laser mirror. This mirror breaks the symmetry of the electron beam line at the location ($z \sim 0.8$ m from the cathode) where the electron beam has a rather large transverse extension and its transverse phase space could be affected by a nonlinear kick. More detailed investigations on this effect have to be done.

The measured optimized phase space for 2 nC has a negative covariance $\langle xx' \rangle$ whereas the simulated phase space is positively correlated (Fig. 8). This could be a consequence of the fact that the experimentally found optimum machine setup (namely the laser spot size at the cathode and the gun launch phase) is quite strongly deviating from the simulated optimum settings. This difference for 2 nC is larger than for the 1 nC case. The experimentally found optimum space charge density [$\sim Q/(\sigma_{xy}^{l})^2$] is increased by 30% when the charge is increased from 1 to 2 nC, whereas the simulated dependency of this density on the bunch charge for optimum cases is much weaker (even a 10% reduction for the charge increase from 1 to 2 nC).

I. Emittance optimization for 0.1 nC

The emittance optimization for 0.1 nC beams is of special interest. Because of the above-mentioned new implementations in the low level rf system (see Sec. II A) the gun phase slope can now be corrected. This resulted in increased equality of the emission phases of the electron bunches within a pulse train which is required for high quality emittance measurements at low charge level. The improved shot-to-shot phase stability has also a larger impact for emittance measurements at low charges because of better pointing stability of significantly smaller electron beams at the location of the slit masks. A set of dipole correcting coils was applied to steer electron bunches to the center of screens used for the emittance measurements and the beam energy jitter caused by rf phase fluctuations immediately impacts the position stability of the electron beam. Besides that a relatively good agreement between measurements and beam dynamics simulations was obtained. It is remarkable that it was possible to reproduce the measured charge in the simulations by applying the experimental machine settings. Measured and simulated rms size and emittance of a 0.1 nC electron beam are shown in Fig. 24 as a function of the main solenoid current (for measurements) and peak field (simulations) detuning. For one set of simulations shown in these plots, the measured laser rms spot size of 0.123 mm was applied, the gun phase was set to deliver the measured maximum mean momentum of 6.71 MeV/c. The gun phase in the simulations was set to the MMMG phase which corresponds to the experimental conditions. The results of the simulations are shown with solid black curves in Fig. 24. These settings differ from the optimum setup obtained from the simulations (see Table I), corresponding simulated curves are shown in Fig. 24 with dashed black lines for comparison. Compared to the 1 nC case, the agreement between the measurements and the experimental data is better for the 0.1 nC bunch charge, although there is a rather strong x-y asymmetry in the experimentally observed electron beams. The measured optimum phase space distribution of the 0.1 nC electron beam is shown in Fig. 25 in comparison with corresponding simulated distribution.

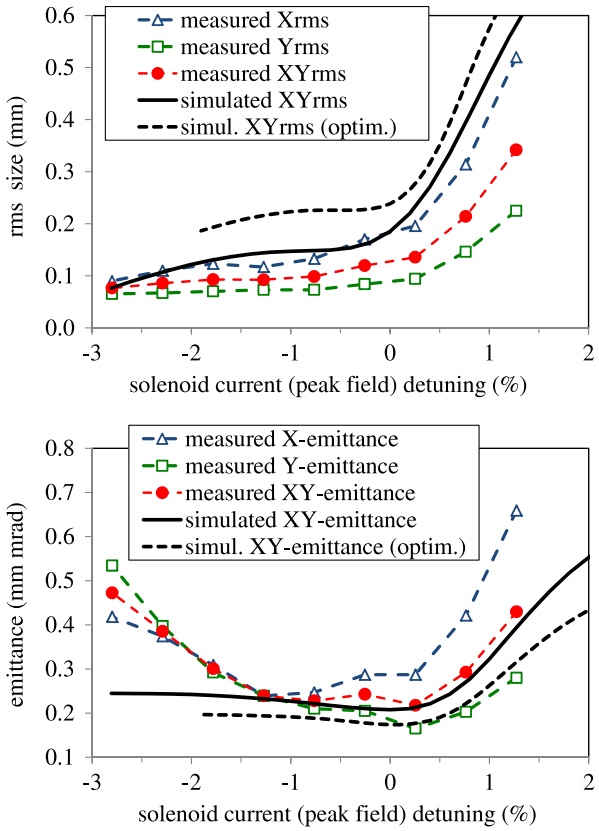

FIG. 24. Measured and simulated rms size (upper plot) and emittance (bottom plot) for 0.1 nC versus main solenoid current detuning. The optimum solenoid current from the experimental data $I^{*}_{\mathrm{main}} = 393$ A corresponds to the simulated optimum peak field of $-0.226\,71$ T. Results of the optimized simulations (see Table I for the parameters) are shown with dashed curves.

J. Core emittance

The procedure for the projected emittance measurement at PITZ is supposed to be as conservative as possible. According to this paradigm, as much as possible electron beam related signal has to be collected and involved in the phase space reconstruction. The image filters applied to the beam and beamlet analysis to separate the beam signal from the dark current background and camera intrinsic noise are designed according to this approach. The emittance values are obtained from these measurements without any assumption concerning the particle distribution function. This procedure results in a conservative estimation of the rms emittance values and the phase space distributions, which contain a significant part of beam particles far distant from the phase space center. Those outlying particles are not expected to play a significant role in the later FEL lasing processes but have a substantial impact on the emittance values. So, one can apply a charge cut procedure to the measured raw phase spaces in order to study the structure of the core emittance and the role of the beam halo. The charge cut is performed by discriminating phase space areas with intensities lower than an introduced

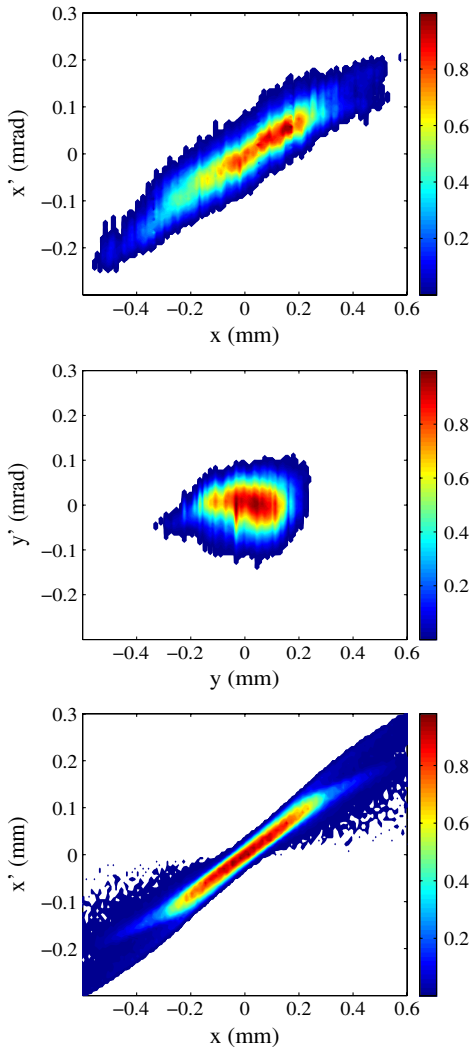

FIG. 25. Measured horizontal (upper plot), vertical (middle plot), and simulated horizontal phase space (bottom plot) for a bunch charge of 0.1 nC. Because of perfect *x*-*y* symmetry assumed in simulations, the simulated vertical phase space is identical to the horizontal one.

threshold, resulting in the new phase space with removed low intensity parts. It contains reduced charge (overall integral) and phase space area (core emittance). Consequently, increasing the intensity threshold in fine steps the rms normalized core emittance can be calculated as a function of the charge cut. This charge cut is independently performed for both measured transverse phase spaces and the resulting emittance values are used to calculate the geometrical mean value for the *xy* emittance obtained for a given charge cut level. The charge cut procedure is illustrated by Fig. 26, where transverse phase spaces experimentally optimized for the 1 nC electron beam are shown. The upper row of plots shows raw measured horizontal and vertical phase spaces (no charge cut performed). The rms normalized emittance values for this case are 0.707 ± 0.032 mm mrad and 0.685 ± 0.024 mm mrad for x and y

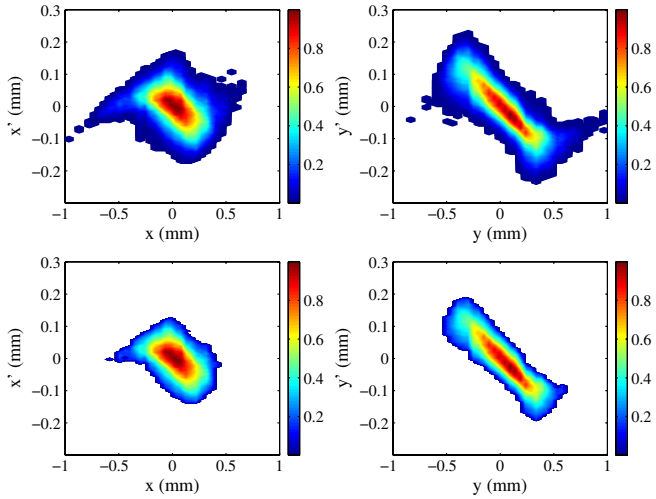

FIG. 26. Measured horizontal (left column) and vertical (right column) phase space for a bunch charge of 1 nC. The upper row corresponds to the raw data (100% of the measured beam signal), whereas the bottom plots are obtained for 90% of measured charge.

planes, respectively. The bottom row of plots shows the results of a 10% charge cut applied to the raw phase spaces. Corresponding emittance values are 0.543 ± 0.025 mm mrad and 0.515 ± 0.017 mm mrad.

The resulting core *xy* emittance measured for various bunch charges is shown in Fig. 27. The charge cut was applied to the measured optimum phase space for each bunch charge. The results of the optimization for the gun operation at the MMMG phase are shown for all charges. Additionally, the charge cut is performed for the results of 2 and 1 nC with gun operation at $+6$ deg (dashed lines in Fig. 27).

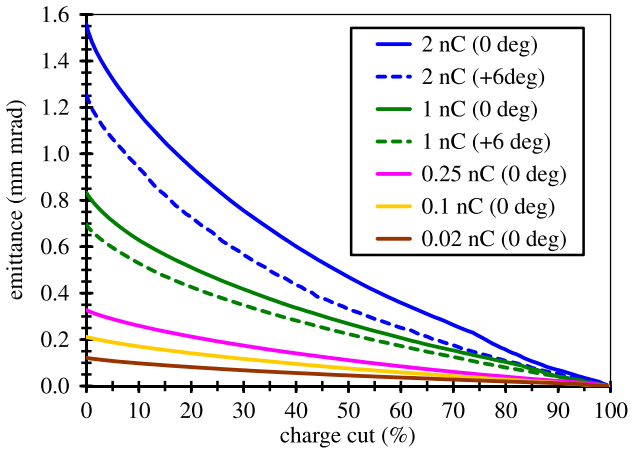

FIG. 27. Measured core *xy* emittance for different charges as a function of the charge cut. A charge cut of 0% corresponds to the emittance values from the raw phase space with full beam signal taken into account. The corresponding gun phase w.r.t. the MMMG phase as used during the measurements is shown in the legend.

TABLE IV. Core xy emittance (mm mrad) measured for various bunch charges and gun phases. Only statistical errors are shown (see text).

Bunch charge	Gun phase	0%	Charge cut 5%	10%	20%
2.0 nC	0 deg	1.558 ± 0.050	1.324 ± 0.045	1.173 ± 0.039	0.936 ± 0.031
2.0 nC	6 deg	1.251 ± 0.064	1.064 ± 0.054	0.939 ± 0.048	0.728 ± 0.037
1.0 nC	0 deg	0.833 ± 0.038	0.711 ± 0.033	0.629 ± 0.029	0.511 ± 0.024
1.0 nC	6 deg	0.696 ± 0.020	0.596 ± 0.017	0.529 ± 0.015	0.427 ± 0.013
0.25 nC	0 deg	0.328 ± 0.010	0.289 ± 0.009	0.260 ± 0.008	0.213 ± 0.006
0.10 nC	0 deg	0.212 ± 0.006	0.188 ± 0.006	0.170 ± 0.006	0.141 ± 0.006
0.02 nC	0 deg	0.121 ± 0.001	0.108 ± 0.001	0.098 ± 0.001	0.082 ± 0.002

Several values of the core emittance obtained from the experimentally optimized phase spaces are summarized in Table IV for various bunch charges and gun phases. Only statistical errors are shown in the table, which are obtained by applying the charge cut procedure to the phase spaces measured by taking consequently 3×3 statistics as explained in Sec. IV A. The systematic errors are typically a factor 3 larger (as it was discussed in Sec. IV G).

V. CONCLUSIONS

In this paper we have described the latest results of the experimental optimization of the high brightness electron source at the Photo Injector Test facility at DESY, Zeuthen site (PITZ). The gun prototype 4.1, operated at a peak cathode electric field of about 60 MV/m, was supplemented with an in-vacuum directional coupler. This made possible an active feedback on the rf gun launch phase. The shot-to-shot phase stability was improved by more than an order of magnitude. A phase slope correction within the rf pulse of up to 700 μs length has enabled efficient measurements of long pulse trains with nearly identical bunches. A new CDS booster cavity has increased the final maximum electron beam momentum up to about 25 MeV/c. These and several other improvements resulted in a significant increase of the photoinjector performance. In 2011 the projected emittance was reduced by about 30% compared to the measurements of the year 2009. The emittance of the electron beam was experimentally optimized for a wide range of bunch charges—from 0.02 to 2 nC. Although the analysis procedure was chosen to be very conservative and 100% rms emittance values are calculated, the gained results are setting a new benchmark for experimentally optimizing photoinjector performance in the whole bunch charge range (see Table IV).

Beam dynamics simulations have been performed in order to study the emittance dependence on various machine parameters. This helped to establish an experimental procedure for the emittance optimization, which has been described in detail. Experimental studies of the emittance dependencies on various photoinjector parameters were presented in comparison with corresponding beam dynamics simulations. Good agreement of measured and simulated electron beam properties was obtained for 0.1 nC bunch charge. Studies for higher bunch charges revealed a discrepancy between optimum experimental machine parameters and results of the optimum simulated setups. The observed discrepancy becomes larger with increasing bunch charge, which indicates space charge effect as the most probable reason. More detailed studies in the vicinity of the photocathode have shown that the mismatch between simulations and measurements can be detected already in the charge production. Further studies are required for a detailed understanding of the beam dynamics of space charge dominated emission from photocathodes in rf guns and for improving the corresponding implementation in beam dynamics simulation programs.

ACKNOWLEDGMENTS

The authors would like to thank the technical groups for their continuous support and all colleagues from the PITZ collaboration for common interest and useful discussions. Special thanks are given to R. Brinkmann for detailed discussion on the emittance results.

[1] W. Ackermann *et al.*, Nature Photon. **1**, 336 (2007).
[2] M. Altarelli *et al.*, DESY, Hamburg Report No. DESY 2006-097, 2007.
[3] P. Schmüser, M. Dohlus, and J. Rossbach, *Ultraviolet and Soft X-Ray Free-Electron Lasers: Introduction to Physical Principles, Experimental Results, Technological Challenges* (Springer-Verlag, Berlin, 2008).
[4] F. Stephan *et al.*, Phys. Rev. ST Accel. Beams **13**, 020704 (2010).
[5] S. Rimjaem *et al.*, Nucl. Instrum. Methods Phys. Res., Sect. A **671**, 62 (2012).
[6] S. Rimjaem *et al.*, in *Proceedings of the 11th European Particle Accelerator Conference* (EPS-AG, Genoa, Italy, 2008), p. 244, MOPC078.
[7] M. Otevrel *et al.*, in Proceedings of 32nd International Free Electron laser Conference (Malmö, Sweden, 2010), WEPB05 [http://accelconf.web.cern.ch/AccelConf/FEL2010/papers/wepb05.pdf].
[8] D. Reschke *et al.*, in Proceedings of the 13th International workshop on RF Superconductivity (Beijing, China,

2007), TUP48 [http://accelconf.web.cern.ch/AccelConf/srf2007/PAPERS/TUP48.pdf].

[9] I. Isaev *et al.*, in *Proceedings of the 2nd International Particle Accelerator Conference* (EPS-AG, Spain, 2011), MOPC154.

[10] V. Paramonov *et al.*, in *Proceedings of the 25th Linear Accelerator Conference* (ICR, Tsukuba, Japan, 2010), MOP081.

[11] I. Will and G. Klemz, Opt. Express **16**, 14922 (2008).

[12] K. Flöttmann, ASTRA particle tracking code [http://www.desy.de/~mpyflo/].

[13] K. Flöttmann, DESY Report No. TESLA-FEL 97-01, Hamburg, 1997.

[14] M. Krasilnikov *et al.*, in *Proceedings of the 21st Particle Accelerator Conference* (IEEE, Knoxville, 2005), WPAP005.

[15] K. J. Kim, Nucl. Instrum. Methods Phys. Res., Sect. A **275**, 201 (1989).

[16] J. Rosenzweig and E. Colby, in *Proceedings of 1995 Particle Accelerator Conference* (IEEE, Dallas, 1995), WPB05 [http://accelconf.web.cern.ch/AccelConf/p95/ARTICLES/WPB/WPB05.PDF].

[17] TTF Photocathodes Database [http://wwwlasa.mi.infn.it/ttfcathodes/].

[18] M. Krasilnikov *et al.*, in Proceedings of 33nd International Free Electron laser Conference (EPS-AG, Shanghai, China, 2011), THPA08.